

Study of Dissipative Collisions of ^{20}Ne ($\sim 7\text{-}11$ MeV/nucleon) + ^{27}Al

Aparajita Dey, C. Bhattacharya, S. Bhattacharya, T. K. Rana, S. Kundu, K. Banerjee, S. Mukhopadhyay,
S. R. Banerjee, D. Gupta, R. Saha

Variable Energy Cyclotron Centre, Sector - 1, Block - AF, Bidhan Nagar, Kolkata - 700 064, India.

The inclusive energy distributions of complex fragments ($3 \leq Z \leq 9$) emitted in the reactions ^{20}Ne (145, 158, 200, 218 MeV) + ^{27}Al have been measured in the angular range $10^\circ - 50^\circ$. The fusion-fission and the deep-inelastic components of the fragment yield have been extracted using multiple Gaussian functions from the experimental fragment energy spectra. The elemental yields of the fusion-fission component have been found to be fairly well explained in the framework of standard statistical model. It is found that there is strong competition between the fusion-fission and the deep-inelastic processes at these energies. The time scale of the deep-inelastic process was estimated to be typically in the range of $\sim 10^{-21} - 10^{-22}$ sec., and it was found to decrease with increasing fragment mass. The angular momentum dissipations in fully energy damped deep-inelastic process have been estimated from the average energies of the deep-inelastic components of the fragment energy spectra. It has been found that, the estimated angular momentum dissipations, for lighter fragments in particular, are more than those predicted by the empirical sticking limit.

PACS number(s): 25.70.Jj, 24.60.Dr, 25.70.Lm

I. INTRODUCTION

Complex fragment emission in heavy-ion induced reactions involving light nuclei ($A_{\text{target}} + A_{\text{projectile}} \lesssim 60$) at bombarding energies well above the Coulomb barrier has been studied quite extensively in the recent years [1–16] to understand the origin of fragment emission and the role of underlying dynamics. It is well known that different types of reaction mechanisms contribute to fragment emission at different energy regions. At bombarding energies near the Coulomb barriers, complete fusion (CF) process is the dominant reaction mechanism. At higher energies, this process is limited by the contributions of other competing processes, such as quasi-elastic (QE) and deep-inelastic (DI) collisions. The CF cross-section increases with incident energy at lower energies and reaches a near-saturation value at higher energies. On the other hand, non-fusion processes become increasingly dominant at higher energies. Thus, the fragments emitted in light heavy-ion collisions at energies well above the Coulomb barrier may have different origins, which extend from partially relaxed processes, such as, quasi-elastic (QE) collision / projectile break-up [17,18], deep-inelastic (DI) transfer and orbiting [8,9,19–22], to fully relaxed fusion-fission (FF) [23–28] process. In some cases, the structure of the nuclei has also been found to play an important role. Therefore, the characterization of the origin of fragments is of utmost importance to extract information on the relaxation of various degrees of freedom (energy and angular momentum dissipation, for example) in heavy ion collision in this energy domain. However, for light systems, the distinction between different reaction mechanisms, FF and orbiting or DI processes in particular, is very difficult as there is strong overlap in the elemental distributions of the fragments emitted in these processes.

Binary decay of the light composite system ^{47}V has been investigated quite extensively in the past years. In some cases, (where the composite system ^{47}V was produced through inverse kinematical reactions, like, $^{35}\text{Cl} + ^{12}\text{C}$ [4,5,29,30], $^{31}\text{P} + ^{16}\text{O}$ [7], $^{23}\text{Na} + ^{24}\text{Mg}$ [6]) it was found that the ^{47}V composite system decays statistically. In these cases, the emitted fragment yields show $1/\sin \Theta_{c.m.}$ - like angular dependence and have angle-independent mean total kinetic energy (TKE) values in agreement with the decay of a fully energy equilibrated composite system. The experimental cross-sections are well explained with the predictions of the extended Hauser-Feshbach method (EHFM) [25] and thus suggest a fusion-fission origin. It was further concluded that orbiting process [9] does not play any significant role in the decay of ^{47}V composite system. On the other hand, studies on the same system, produced through direct kinematical reactions ($^{20}\text{Ne} + ^{27}\text{Al}$ [31–33]), showed that the angular distributions of fully damped fragments are forward peaked and fall off faster than $1/\sin \Theta_{c.m.}$, which are characteristic of DI processes. Subsequently, assuming the fragment yield to be of DI origin (and assuming the sticking limit for the angular momentum dissipation), a highly elongated configuration for the $^{20}\text{Ne} + ^{27}\text{Al}$ di-nuclear system was conjectured [32].

It is clearly evident from the above that some degree of ambiguity prevails over the interpretation of the fragment yield data in the decay of ^{47}V composite system. To resolve the ambiguity, it is necessary to understand the roles played by various competing processes in this energy regime. For example, there is strong competition between FF and DI processes at these energies, which should be deciphered properly to extract meaningful information about the reaction mechanism. In recent years, we have developed a scheme for the decomposition of FF and DI components of the fragment yield [14,20] in order to study systematically the competition between FF and DI processes in light heavy ion collisions at energies well above the barrier; In this paper, we report an experimental study of fragment

emission in the decay of ^{47}V composite system, produced through ^{20}Ne (145 – 218 MeV) + ^{27}Al reactions. Some part of the ^{20}Ne (145 MeV) + ^{27}Al data has already been published [20]. The FF and DI components of the fragment yields have been extracted in each case to study the systematics of the two processes in the above energy range.

The paper has been arranged as follows. The experimental procedures are given in the next section. The experimental results are presented in Sec. III. Finally, The discussion and conclusion are given in Sec. IV.

II. EXPERIMENTAL PROCEDURES

The experiments have been performed using the accelerated ^{20}Ne ion beams from the Variable Energy Cyclotron at Kolkata. The beam energies were 145, 158, 200 and 218 MeV; the target was made of self-supporting ^{27}Al of thickness $\sim 515 \mu\text{g}/\text{cm}^2$. Fragments have been detected using two types of solid state telescopes; telescopes with $\sim 10 \mu\text{m} \Delta E$ [Si(SB)], $300 \mu\text{m} E$ [Si(SB)] were used to detect heavier fragments ($5 \leq Z \leq 9$), whereas telescopes with $\sim 10 \mu\text{m} \Delta E$ [Si(SB)], $5 \text{ mm} E$ [Si(Li)] were used for the detection of lighter fragments ($3 \leq Z \leq 5$). The two types of telescopes were mounted on two arms of the scattering chamber which could move independently. Typical solid angle subtended by each detector was $\sim 0.6 \text{ msr}$. The telescopes were calibrated using elastically scattered ^{20}Ne ion from Au, Al targets and Th- α source. The systematic errors in the data, arising from the uncertainties in the measurements of solid angle, target thickness and the calibration of current digitizer have been estimated to be $\approx 15\%$.

III. EXPERIMENTAL RESULTS

A. Energy distribution

The inclusive energy distributions have been measured for the fragments ($3 \leq Z \leq 9$) emitted in the reaction $^{20}\text{Ne} + ^{27}\text{Al}$ at the bombarding energies 145, 158, 200 and 218 MeV, respectively, in the angular range $10^\circ - 50^\circ$. Typical fragment energy spectra (at $\theta_{lab} = 15^\circ$) have been displayed in Fig. 1 for different bombarding energies. It is evident from Fig. 1 that the shapes of the energy spectra of the heavier fragments (viz., F) are quite different from those of the lighter fragments, viz., B and C at all bombarding energies. It is mainly due to the variation of the relative contributions of DI and FF processes for different fragments. The contributions of FF and DI components have been estimated by fitting the measured energy spectra with Gaussian functions as per the procedure laid down in Ref. [14]. The energy spectra of different fragments at each angle have been fitted with two Gaussian functions in two steps. In the first step, the FF component of the fragment energy distribution has been extracted in the following way; The energy distribution of the FF component was taken to be a Gaussian. The centroid of the Gaussian was obtained from Viola systematics [34,35], adapted for light nuclear systems [36], of total kinetic energies of mass-symmetric fission fragments duly corrected for asymmetric factor [15]. The FF component of the energy spectrum thus obtained was then subtracted from the full energy spectrum. In the next step, the DI component was obtained by fitting the subtracted energy spectrum with a second Gaussian. This is illustrated in Fig. 1, where the extracted FF (dashed curve) and DI (dash-dotted curve) components have been displayed along with the experimental data for all bombarding energies. It is clear from Fig. 1 that the experimental energy spectra, for all fragments at all bombarding energies, may be explained fairly well as sum of two Gaussian functions representing the FF and DI components (sum of FF and DI are shown by solid curve). In each spectrum, the arrow at lower energy corresponds to the centroid of the Gaussian for the FF component and the arrow at higher energy corresponds to the centroid of the Gaussian for the DI component.

B. Angular distribution

The FF and the DI components of the fragment angular distributions have been obtained by integrating the respective energy distributions. The center-of-mass (c.m.) angular distributions of the FF components of various fragments for all bombarding energies have been displayed as a function of c.m. angle ($\Theta_{c.m.}$) in Fig. 2. The transformation from the laboratory system to the c.m. system has been done with the assumption of a two-body kinematics averaged over total kinetic energy distributions. The angular distributions of FF components exhibit $d\sigma/d\Omega \sim 1/\sin \Theta_{c.m.}$ -like dependence (solid lines in Fig. 2), which are in conformity with the systematics of fission decay of a fully equilibrated system.

The c.m. angular distributions of the DI components of different fragments for all bombarding energies have been displayed as a function of c.m. angle in Fig. 3. A rapid fall of the angular distribution, (faster than $d\sigma/d\Omega \sim$

$1/\sin \Theta_{c.m.}$), indicates a shorter lifetime of the composite system. Such lifetimes are incompatible with the formation of an equilibrated compound nucleus, but may still reflect significant energy damping within a deep-inelastic mechanism. From the measured forward peaked angular distribution, it is possible to estimate the lifetime of the intermediate dinuclear complex using a diffractive Regge-pole model [15,37]. The angular distributions have been fitted with the following expression:

$$\frac{d\sigma}{d\Omega} \propto \frac{C}{\sin \Theta_{c.m.}} e^{-\Theta_{c.m.}/\Theta_o}, \quad (1)$$

where, Θ_o is called the “life angle”, which is the angle of rotation of the dinuclear composite during the time interval between its formation to the decay into two fragments. The fit to the DI angular distribution with Eq. 1 has been shown in Fig. 3 (solid line). The values of Θ_o thus obtained are given in Table I.

C. Average Q-value distribution

The average Q-value, $\langle Q \rangle$, has been estimated from the total average kinetic energy of the fragments, E_K^{tot} , using the relation, $E_K^{tot} = E_{c.m.} + \langle Q \rangle$. The fragment total average kinetic energies in the center-of-mass have been obtained from the respective laboratory values assuming two body kinematics. The variations of $\langle Q \rangle$ with center-of-mass emission angle for the fragments ($3 \leq Z \leq 9$) obtained at different bombarding energies have been displayed in Figs. 4 and 5. The fragment kinetic energies were appropriately corrected for particle evaporation from the excited primary fragments assuming thermal equilibrium of the dinuclear composite system. It is observed that for all the fragments at all energies, the average Q-values corresponding to FF components are independent of the center-of-mass emission angles, as expected [see Fig. 4]. The average Q-values for DI components have been displayed in Fig. 5. The $\langle Q \rangle$ values for DI components for the fragments Li, Be and B are found to be nearly constant as a function of angle for all bombarding energies, whereas those for C to F are found to decrease at forward angles ($\Theta_{c.m.} \lesssim 40^\circ$) and then they gradually tend to become constant; these imply that, beyond this point, the kinetic energy damping is complete and dynamic equilibrium has been established before the scission of the dinuclear composite takes place.

D. Average velocity

The average velocities of the FF component of the fragments have been computed from their respective centroid energies. The mass number, A , of the fragments have been estimated from the respective experimentally obtained Z values using the empirical relation [38]:

$$A = Z \times (2.08 + 0.0029 \times Z). \quad (2)$$

The average velocities have been plotted in the v_{\parallel} vs. v_{\perp} plane for two representative fragments (Li and O) in Fig. 6, where the measured average velocities of the FF components were denoted by solid symbols and the corresponding v_{CN} was represented by arrow. It is seen that the average velocities fall on a circle (solid curve) centered around v_{CN} , the compound nucleus velocity. This means that the average velocities (as well as kinetic energies) of the fragments are independent of the c.m. emission angles at all incident energies considered here. This clearly indicates that these fragments are emitted from a fully equilibrated compound nucleus emission source with full momentum transfer. The magnitude of the average fragment velocities (*i.e.*, the radii of the circles in Fig. 6) decreases with the increase of fragment mass, which is indicative of the binary nature of the emission.

The average velocities of the DI components at different bombarding energies have also been plotted in Fig. 6 (open symbols) for the same fragments Li and O. It is found that for this component also the average velocities of all fragments fall on a circle (dashed curve) but centered around a higher velocity source (v_{DI}). The values of v_{CN} and v_{DI} for all bombarding energies are given in Table II. It is interesting to note that at each bombarding energy, all DI fragments (only Li and O are shown in figure) are emitted from the same source moving with velocity v_{DI} . Thus the emission of DI fragments, may also be, like FF fragments, visualized in terms of emission from an equilibrated intermediate velocity source.

E. Total elemental yield

The total fusion-fission (σ_{FF}) and deep-inelastic (σ_{DI}) cross-sections for different fragments have been obtained by integrating the respective double differential cross-section ($d^2\sigma/d\Omega dE$) over the whole energy and angular range. The cross-sections thus obtained for different fragments at different bombarding energies have been displayed in Fig. 7 as a function of fragment charge Z . Total uncertainties in the estimation of σ_{FF} and σ_{DI} are due to the experimental threshold and the limited angular range of the data (error bars in Fig. 7). The total elemental yields of the FF components (σ_{FF}) have been compared with the theoretical estimates of the same obtained from the statistical model code CASCADE [39], and, from the extended Hauser-Feshbach method (EHFM) [25]. The model calculations have been performed by using the critical angular momentum value for the respective bombarding energy. The experimental fragment emission cross-sections for FF component are shown in Fig. 7 (left) by filled symbols and the theoretical estimates of the same are represented by solid (CASCADE) and dashed (EHFM) histograms. It is seen from the figure that the theoretical predictions are in fair agreement with the experimental results except for $Z = 4$ fragment, where the experimental values are much smaller than the respective theoretical estimates; this might be because of non-detection of particle unstable ^8Be , which decays (into two α -particles) almost immediately after production and thus escapes detection. The total elemental yield of the DI component (σ_{DI}) are shown in Fig. 7 (right) by open symbols. It has been found that a large fraction of the heavier fragment (C,N,O,F) yield is due to the DI mechanism for all the bombarding energies. The ratio of DI cross-section to FF cross-section increases with bombarding energy (Table III). However, the FF and DI processes are comparable in this bombarding energy range.

IV. DISCUSSION AND CONCLUSION

A. Time scale

The time scale of DI process can be estimated from DI angular distribution using Eq. 1, which describes the decay of a rotating dinucleus with an angular velocity $\omega = \hbar l / \mu R^2$, where μ represents the reduced mass of the system, l is the angular momentum [$l_{cr} < l \lesssim l_{gr}$; l_{cr} , l_{gr} being the critical angular momentum for fusion and the grazing angular momentum, respectively], R represents the distance between the two centers of the dinucleus, and τ is the time interval during which the two nuclei remain in solid contact in the form of the rotating dinucleus. The ‘‘life angle’’ (Θ_o) is then the product of angular velocity (ω) and the rotation time (τ). The characteristics of a reaction process depends on the value of Θ_o . Smaller values of Θ_o are associated with faster processes for which the corresponding angular distributions are more forward peaked. Large values of Θ_o ($\geq 2\pi$) are associated with slow processes with lifetime large or comparable to the dinucleus rotation period $\tau_{rot}(= 2\pi/\omega)$, the value of which lies typically in the range of $\sim 1-2 \times 10^{-21}$ sec. In these cases, long-lived configurations are assumed to be formed and the angular distributions tend to become symmetric around 90° in the c.m. ($d\sigma/d\Omega \sim 1/\sin \Theta_{c.m.}$ type distribution). The FF process is thus a limiting case of DI process, where a very long-lived configuration is assumed to be formed and the angular distribution becomes $\propto 1/\sin \Theta_{c.m.}$. The c.m. angular distributions of DI component have been fitted with Eq. 1 and the time scales thus obtained are given in Table I for different fragments emitted in the $^{20}\text{Ne} + ^{27}\text{Al}$ reactions. The upper (lower) limit of τ corresponds to the estimate with $l = l_{cr}$ (l_{gr}). The values of time scales are found to vary in the range of $10^{-21} - 10^{-22}$ sec., depending on the bombarding energy and fragment mass. It has been found that the time scale decreases as the fragment charge increases. For lower mass fragments (Li to B), the time scale decreases with the bombarding energy also and for other fragments (C to F) it is almost independent of bombarding energy. This is expected because the heavier fragments (near to the projectile) requires less number of nucleon transfer and therefore lesser time. On the other hand, the emission of lighter fragments requires more number of nucleon exchanges and therefore longer time.

B. Angular momentum dissipation

In addition to kinetic energy dissipation, the dissipative heavy ion collision processes also result in significant dissipation of relative angular momentum in the entrance channel. Phenomenologically, the kinetic energy dissipation originates from the radial and tangential component of friction between the surfaces of the rotating dinuclear system; On the other hand, the angular momentum dissipation is decided solely by the tangential component of the friction, and the magnitude of dissipation is expected to lie within any of the two phenomenological limits (rolling and sticking). However, very large dissipation of relative angular momentum in excess of the sticking limit predictions has also been reported in the literature [20,22]. This anomaly may be due to the ambiguity in the determination of the magnitude of

angular momentum dissipation (and vis-à-vis the rotational contribution to the fragment kinetic energy). Moreover, the estimation of the angular momentum in the exit channel is strongly dependent on the scission configuration of the rotating dinuclear system. An independent estimation of the scission configuration is necessary to estimate the angular momentum transfer properly. Generally, it is estimated from the total kinetic energy of the rotating dinuclear system, E_K^{tot} , which is given by,

$$E_K^{tot} = V_N(d) + f^2 \frac{\hbar^2 l_i (l_i + 1)}{2\mu d^2}, \quad (3)$$

where $V_N(d)$ is the contribution from Coulomb and nuclear forces at dinuclear separation distance d , μ is the reduced mass of the dinuclear configuration, l_i is the relative angular momentum in the entrance channel and f is the numerical factor denoting the fraction of the angular momentum transferred depending on the strength of tangential friction. In absence of any method to estimate the values of f and d independently, in an earlier investigation [32,33] f was assumed to be equal to its limiting value (corresponding to the sticking limit) and whole of the fragment yield was assumed to be of DI origin to arrive at an extended dinuclear configuration for $^{20}\text{Ne} + ^{27}\text{Al}$ system. However, we have demonstrated [Ref. [14,20] and present paper] that, at these energies, a significant part of the fragment yield is of FF origin and therefore this part should be subtracted from the total yield to properly estimate the DI yield. The extracted FF and DI yields can be utilized to estimate the values of d and f . A simple procedure for estimating both d and f was given in Ref. [20]. Deep inelastic collisions are believed to occur within the angular momentum window between the critical angular momentum for fusion, l_{cr} and the grazing angular momentum, l_{gr} . The partially dissipative part of it (DI at forward angles) originates in near peripheral collisions ($l \sim l_{gr}$), which correspond to small overlap and a fairly elongated dinuclear configuration; On the other hand, fully energy equilibrated dissipative components (at larger angles) correspond to more compact collisions near $l \sim l_{cr}$. Moreover, the fusion-fission yield is also most predominant in the vicinity of $l \sim l_{cr}$. It is, therefore, likely that the exit channel configurations of both the processes are similar and it appears to be reasonable to assume a compact scission shape for the fully energy damped component of the DI yield. In the present work, we estimated the scission configuration from the extracted fusion-fission component of the measured fragment energy spectra. The separation distance d between the two fragments at the scission point is calculated from the energy centroid of the FF energy spectra. The mean values of d thus estimated are 7.7 ± 1.2 fm for $^{20}\text{Ne} + ^{27}\text{Al}$ reaction. Assuming these scission configurations, Eq. 3 may then be used to extract the angular momentum dissipation factor, f , in the case of fully energy damped DI collisions. The values of f extracted for different energies for $^{20}\text{Ne} + ^{27}\text{Al}$ reaction are displayed in Fig. 8 alongwith the rolling (solid line) and sticking (dashed line) limit predictions for the same. During the calculation the value of initial angular momentum l_i was taken to be equal to the critical angular momentum for fusion, l_{cr} .

It is apparent from Fig. 8 that for all the reactions considered, there is discrepancy between the experimental and empirical estimates of angular momentum dissipation; so far as the lighter fragments ($Z = 3 - 5$) are concerned. For these fragments, the experimental estimates of angular momentum dissipation are more than their limiting values predicted under the rolling and sticking conditions. The discrepancy is more for low mass fragments, and gradually decreases for heavier fragments. This may be qualitatively understood as follows: it is known from the study of dissipative dynamics of fission [40] that, strong frictional forces in the exit channel causes considerable retardation of the scission process leading to increase in scission time scale. As the the exit channel configurations of the fully damped DI process are taken to be similar to those for FF process (except that the dinuclear system, in case of DI collision, is formed beyond the conditional saddle point directly), the dynamics of DI process may also experience stronger frictional forces. Microscopically, friction is generated due to stochastic exchange of nucleons between the reacting partners through the window formed by the overlap of the density distributions of the two. Stronger friction, in this scenario, essentially means larger degree of density overlap and more nucleon exchange. Consequently, lighter DI fragments (corresponding to more net nucleon transfer) originate from deeper collisions, for which interaction times are larger. Therefore, the angular momentum dissipation, originating due to stochastic nucleon exchange, may also be more which, at least qualitatively, explains the observed trend. The angular momentum dissipation for a particular fragment (*e.g.*, Li, Be, B) is found to be nearly independent of the bombarding energy. This is clearly shown from Fig. 9 where the factor f have been displayed as a function of bombarding energy for the $^{20}\text{Ne} + ^{27}\text{Al}$ reaction. This may be further indicative of the stochastic nucleon exchange origin of the frictional force for the fully energy damped DI process, for which scission configuration is nearly independent of the bombarding energy.

To summarise, We have studied ^{20}Ne (145, 158, 200, 218 MeV) + ^{27}Al reactions and extracted the contributions to the fragment yield from fusion-fission and deep inelastic processes. The c.m. angular distributions of FF component was found to have $\sim 1/\sin \Theta_{c.m.}$ dependence whereas those of DI component showed an exponential fall off at forward angles. The time scale of the DI process has been estimated form the DI angular distribution. The lifetime of DI process has been found to decrease with increasing fragment mass and also with increasing bombarding energy. The fusion-fission component of the emitted fragments has been found to be originate from the compound nucleus source

(moving with velocity v_{CN}), while the deep inelastic component of the fragments are found to be emitted from an intermediate velocity source having velocity v_{DI} , which is higher than v_{CN} . The average Q-values for DI component have been found to decrease with increase of emission angles and saturate at higher angles signifying fully energy damped process at these angles; On the other hand, those for FF component have been found to be independent of emission angles as expected in equilibrium emission. The elemental cross-sections have been obtained by integrating separately the energy distributions of the FF and DI components over the corresponding energies and over the whole angular range. The fusion-fission fragment yield, σ_{FF} , have been found to be fairly well explained in terms of statistical model. The σ_{DI}/σ_{FF} value increases with bombarding energies, which is expected because of increasing contribution of DI processes at higher energies. Assuming a compact exit channel configuration (estimated from extracted FF part of the spectra) for the fully damped part of the deep-inelastic reactions, the angular momentum dissipation has been estimated and it has been found to be more than the corresponding phenomenological limits. The deviations are found to be more for lighter fragments, which may be related to the microscopic (stochastic nucleon exchange) origin of nuclear friction.

ACKNOWLEDGMENTS

The authors like to thank the cyclotron operating crew for smooth running of the machine, and H. P. Sil for the fabrication of thin silicon detectors for the experiment. One of the authors (A. D.) acknowledges with thanks the financial support provided by the Council of Scientific and Industrial Research, Government of India.

-
- [1] S. J. Sanders, A. Szanto de Toledo, and C. Beck, Phys. Rep. **311**, 487 (1999) and references therein.
 - [2] S. J. Sanders, D. G. Kovar, B. B. Back, C. Beck, B. K. Dichter, D. Henderson, R. V. F. Janssens, J. G. Keller, S. Kaufman, T. F. Wang, B. Wilkins, and F. Videback, Phys. Rev. Lett. **59**, 2856 (1987).
 - [3] Sl. Cavallaro, G. Prete, and G. Viesti, Phys. Rev. C **41**, 1606 (1990).
 - [4] C. Beck, B. Djerroud, B. Heusch, R. Dayras, R. M. Freeman, F. Haas, A. Hachem, J.P. Wieleczko, and Y. Youlal, Z. Phys. A **334**, 521 (1989).
 - [5] C. Beck, B. Djerroud, F. Haas, R. M. Freeman, A. Hachem, B. Heusch, A. Morsad, M. Youlal, Y. Abe, R. Dayras, J. P. Wieleczko, T. Matsuse, and S. M. Lee, Z. Phys. A **343**, 309 (1992).
 - [6] C. Beck, D. Djerroud, F. Haas, R. M. Freeman, A. Hachem, B. Heusch, A. Morsad, M. Vuillet-A-Cilles, and S.J. Sanders, Phys. Rev. C **47**, 2093 (1993).
 - [7] A. Ray, D. Shapira, J. Gomez del Campo, H. J. Kim, C. Beck, B. Djerroud, B. Heusch, D. Blumenthal, and B. Shivakumar, Phys. Rev. C **44**, 514 (1991).
 - [8] D. Shapira, R. Novotny, Y. C. Chan, K. A. Erb, J. L. C. Ford, Jr., J. C. Peng, and J. D. Moses, Phys. Lett. **114B**, 111 (1982).
 - [9] B. Shivakumar, S. Ayik, B.A. Harmon, and D. Shapira, Phys. Rev. C **35**, 1730 (1987).
 - [10] B. Shivakumar, D. Shapira, P. H. Stelson, S. Ayik, B. A. Harmon, K. Teh, and D. A. Bomley, Phys. Rev. C **37**, 652 (1988).
 - [11] A. T. Hasan, S. J. Sanders, K. A. Farrar, F. W. Prosser, B. B. Back, R. R. Betts, M. Freer, D. J. Henderson, R. V. F. Janssens, A. H. Wuosmaa, and A. Szanto de Toledo, Phys. Rev. C **49**, 1031 (1994).
 - [12] K. A. Farrar, *et al.*, Phys. Rev. C **54**, 1249 (1996).
 - [13] R. M. Anjos, N. Added, N. Carlin, L. Fante, Jr., M. C. S. Figueira, R. Matheus, H. R. Schelin, E. M. Szanto, C. Tenreiro, A. Szanto de Toledo, and S. J. Sanders, Phys. Rev. C **48**, R2154 (1993).
 - [14] C. Bhattacharya, K. Mullick, S. Bhattacharya, K. Krishan, T. Bhattacharjee, P. Das, S. R. Banerjee, D. N. Basu, A. Ray, S. K. Basu, and M. B. Chatterjee, Phys. Rev. C **66**, 047601 (2002).
 - [15] C. Beck, *et al.*, Eur. Phys. J. A **2**, 281 (1998).
 - [16] Sl. Cavallaro, E. De Filippo, G. Lanzano, A. Pagano, and M. L. Sperduto, Phys. Rev. C **57**, 731 (1998).
 - [17] N. Carlin-Filho, *et al.*, Phys. Rev. C **40**, 91 (1989).
 - [18] S. J. Padalino, *et al.*, Phys. Rev. C **41**, 594 (1990).
 - [19] C. Bhattacharya, *et al.*, Phys. Rev. C **72**, 011601R (2005).
 - [20] C. Bhattacharya, *et al.*, Phys. Rev. C **69**, 024607 (2004).
 - [21] D. Shapira, J. L. C. Ford, Jr., J. Gomez del Campo, R. G. Stokstad and R. M. Devries, Phys. Rev. Lett., **43**, 1781 (1979).
 - [22] D. Shapira, J. L. C. Ford, Jr. and J. Gomez del Campo, Phys. Rev. C **26**, 2470 (1982).
 - [23] L. G. Moretto, Nucl. Phys. **A247**, 211 (1975).
 - [24] S. J. Sanders, Phys. Rev. C **44**, 2676 (1991).

- [25] T. Matsuse, C. Beck, R. Nouicer, and D. Mahboub, Phys. Rev. C **55**, 1380 (1997).
[26] A. K. Dhara, C. Bhattacharya, S. Bhattacharya, and K. Krishan, Phys. Rev. C **48**, 1910 (1993).
[27] A. Szanto de Toledo, S. J. Sanders, and C. Beck, Phys. Rev. C **56**, 558 (1997).
[28] A. Szanto de Toledo, B. V. Carlson, C. Beck, and M. Thoennessen, Phys. Rev. C **54**, 3290 (1996).
[29] S. Pirrone, S. Aiello, N. Arena, Seb. Cavallaro, S. Femino', G. Lanzalone, G. Politi, F. Porto, S. Romano, and S. Sambataro, Phys. Rev. C **55**, 2482 (1997).
[30] C. Beck, *et al.*, Phys. Rev. C **54**, 227 (1996).
[31] R. L. Kozub, *et al.*, Phys. Rev. C **11**, 1497 (1975).
[32] J. B. Natowitz, M. N. Namboodri, R. Eggers, P. Gonthier, K. Geoffroy, R. Hanus, C. Towsley, and K. Das, Nucl. Phys. **A277**, 477 (1977).
[33] Nguyen Van Sen, R. Darves-Blanc, J. C. Gondrand, and F. Merchez, Phys. Rev. C **27**, 194 (1983).
[34] V. E. Viola, K. Kwiatkowski, and M. Walker, Phys. Rev. C **31**, 1550 (1985).
[35] C. Beck, *et al.*, Phys. Rev. C **54**, 227 (1996).
[36] C. Beck and A. Szanto de Toledo, Phys. Rev. C **53**, 1989 (1996).
[37] T. Mikumo, *et al.*, Phys. Rev. C **21**, 620 (1980).
[38] R. J. Charity *et al.*, Nucl. Phys. **A476**, 516 (1988).
[39] F. Pühlhofer, Nucl. Phys. **A280**, 267 (1977).
[40] A. K. Dhara, K. Krishan, C. Bhattacharya and S. Bhattacharya, Phys. Rev. C **57**, 2453 (1998) and references therein.

TABLE I. The time scales for emission of different DI fragments. The upper (lower) limit corresponds to l_{cr} (l_{gr}). The numbers in brackets denote corresponding uncertainties.

E_{lab} (MeV)	l_{cr} (\hbar)	l_{gr} (\hbar)	Fragment	Θ_o (radian)	τ (10^{-22} s)
145	37	51	Li	7.68(1)	20.85(3) - 15.13(2)
			Be	1.99(1)	5.94(2) - 4.31(2)
			B	0.67(2)	2.16(7) - 1.57(5)
			C	0.43(1)	1.44(3) - 1.04(3)
			N	0.31(1)	1.10(3) - 0.80(2)
			O	0.22(1)	0.82(3) - 0.59(3)
			F	0.21(1)	0.82(4) - 0.60(2)
158	38	54	Li	3.36(1)	8.88(3) - 6.25(2)
			Be	1.76(1)	5.11(3) - 3.60(2)
			B	1.10(1)	3.46(3) - 2.43(2)
			C	0.54(2)	1.76(6) - 1.24(4)
			N	0.47(1)	1.62(3) - 1.14(2)
			O	0.35(2)	1.26(8) - 0.89(5)
			F	0.18(2)	0.68(8) - 0.48(5)
200	41	63	Li	3.09(1)	7.57(2) - 4.93(1)
			Be	1.59(5)	4.29(12) - 2.79(8)
			B	0.98(2)	2.85(6) - 1.85(4)
			C	0.53(2)	1.60(6) - 1.04(4)
			N	0.36(1)	1.15(3) - 0.75(2)
			O	0.32(2)	1.07(6) - 0.70(4)
			F	0.24(3)	0.84(9) - 0.55(7)
218	42	66	Li	1.37(2)	3.28(4) - 2.09(3)
			Be	1.14(1)	3.00(2) - 1.90(2)
			B	0.99(1)	2.81(3) - 1.79(2)
			C	0.56(2)	1.65(6) - 1.05(4)
			N	0.52(1)	1.62(3) - 1.03(2)
			O	0.30(2)	0.98(6) - 0.62(3)
			F	0.24(1)	0.82(4) - 0.52(2)

TABLE II. The values of different velocity sources.

E_{lab} (MeV)	v_{CN} (v/c)	v_{DI} (v/c)
145	0.053±0.001	0.061±0.003
158	0.055±0.001	0.067±0.002
200	0.062±0.001	0.074±0.002
218	0.065±0.001	0.085±0.003

TABLE III. The σ_{DI}/σ_{FF} values for different fragments at all bombarding energies.

E_{lab} (MeV)	σ_{DI}/σ_{FF}				
	C	N	O	F	
145	0.51±0.10	0.52±0.11	0.93±0.17	0.58±0.12	
158	1.20±0.24	1.11±0.22	1.11±0.22	1.47±0.29	
200	1.21±0.23	1.14±0.23	1.20±0.24	1.28±0.26	
218	1.25±0.25	1.15±0.23	1.65±0.33	1.22±0.23	

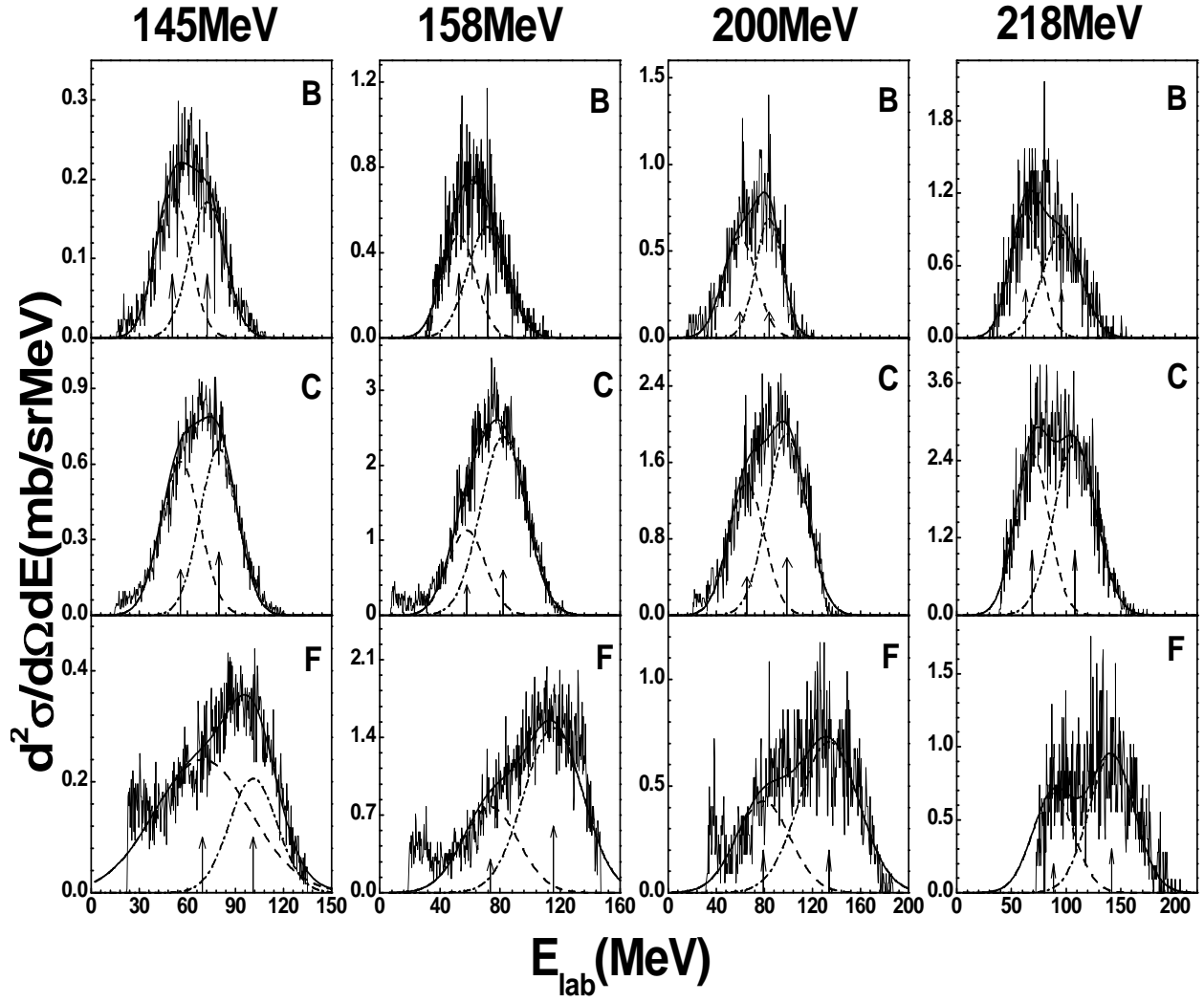


FIG. 1. Inclusive energy distributions for different fragments emitted in $^{20}\text{Ne} + ^{27}\text{Al}$ reaction at different bombarding energies at an angle $\theta_{lab} = 15^\circ$. The FF, DI components and the sum (FF + DI) are denoted by dashed, dash-dotted and solid curves, respectively. The arrows indicate the centroids of the fitted Gaussians.

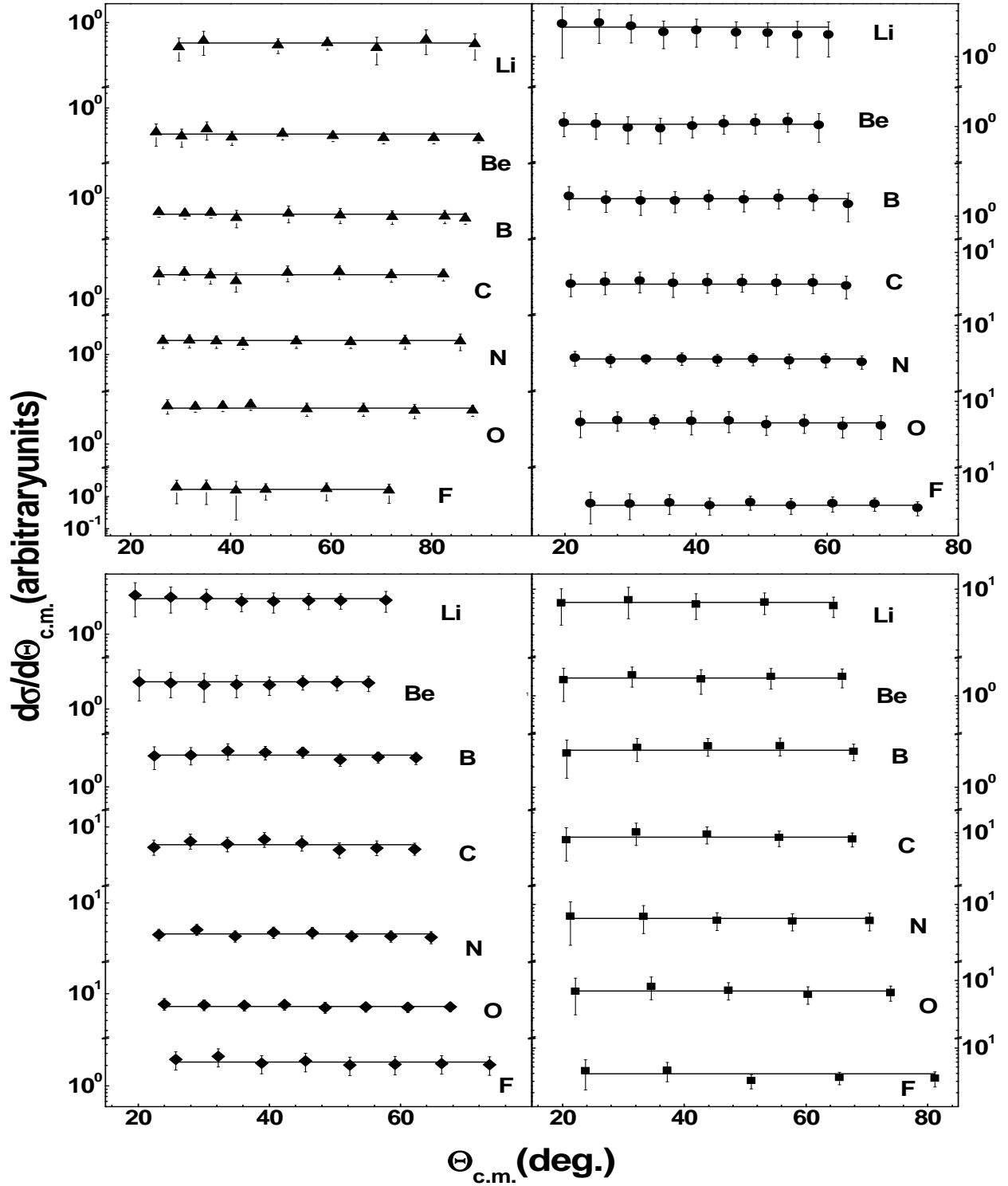


FIG. 2. The c.m. angular distributions of the fusion-fission component for different fragments at the bombarding energies 145 MeV (triangle), 158 MeV (circle), 200 MeV (diamond) and 218 MeV (square). The lines correspond to fission-like angular distribution ($d\sigma/d\Omega \sim 1/\sin \Theta_{c.m.}$) fit to the data.

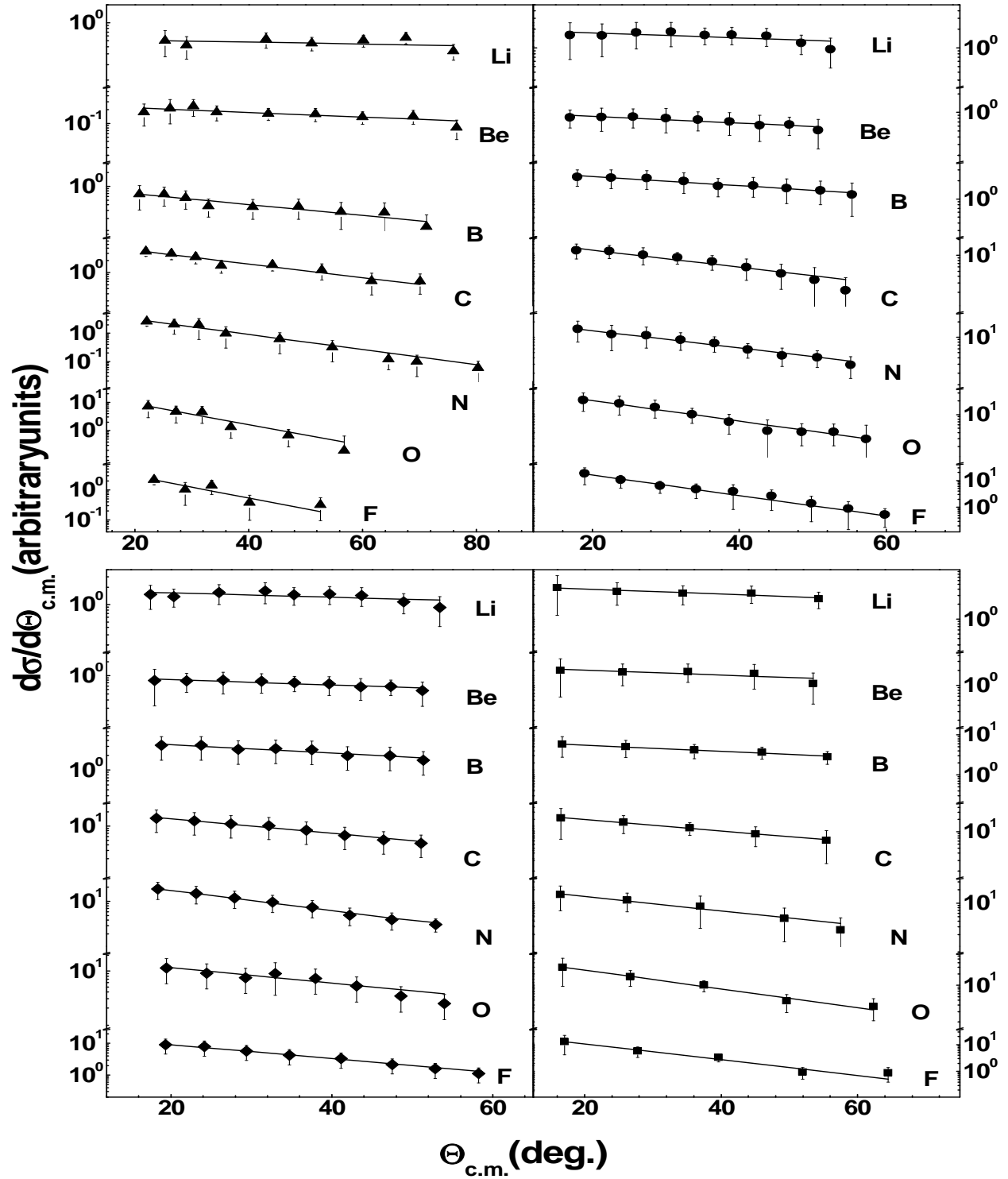


FIG. 3. The c.m. angular distributions of the deep-inelastic component for different fragments at the bombarding energies 145 MeV (triangle), 158 MeV (circle), 200 MeV (diamond) and 218 MeV (square). The lines are exponential fit [Eq. 1] to the data.

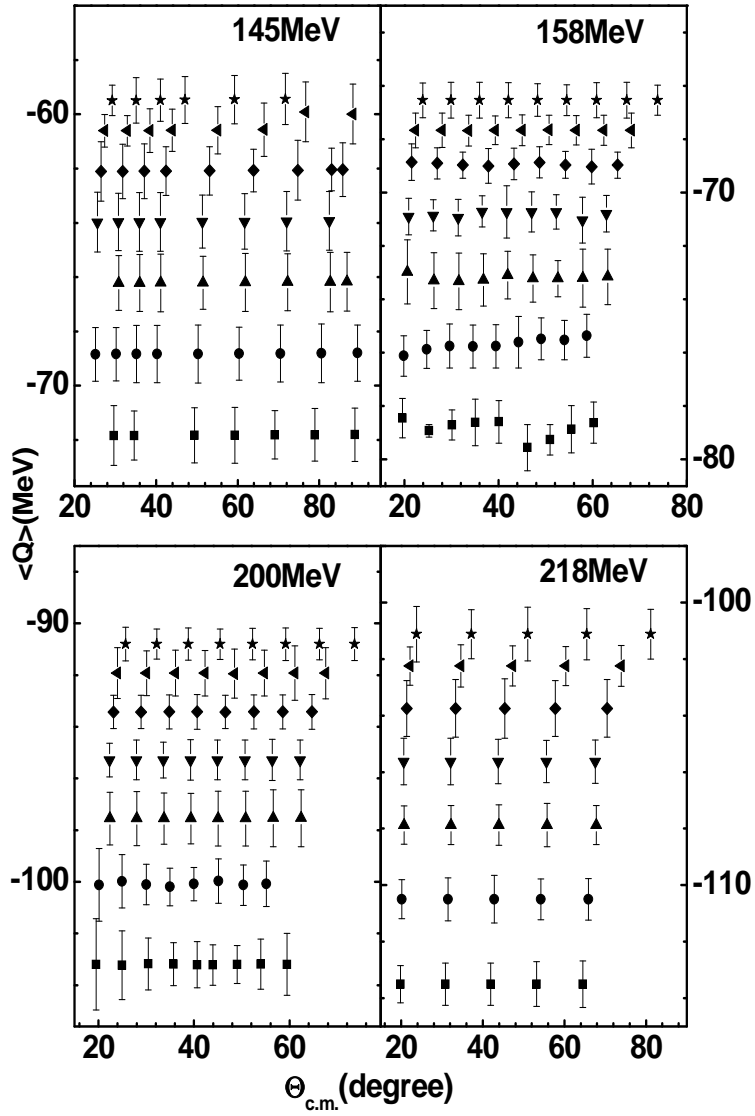


FIG. 4. The average Q -values of the fusion-fission component for the fragments Li(square), Be(circle), B(triangle), C(inverted triangle), N(diamond), O(left triangle) and F(star) at each bombarding energy.

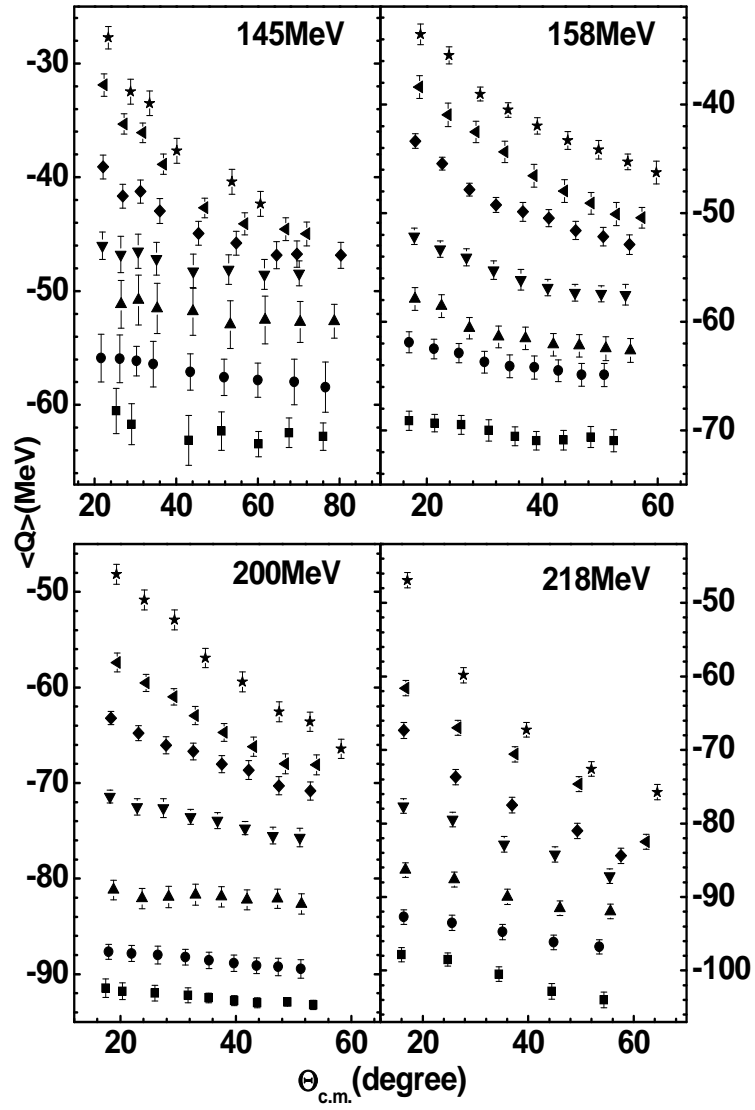


FIG. 5. Same as Fig. 4 for the deep-inelastic component.

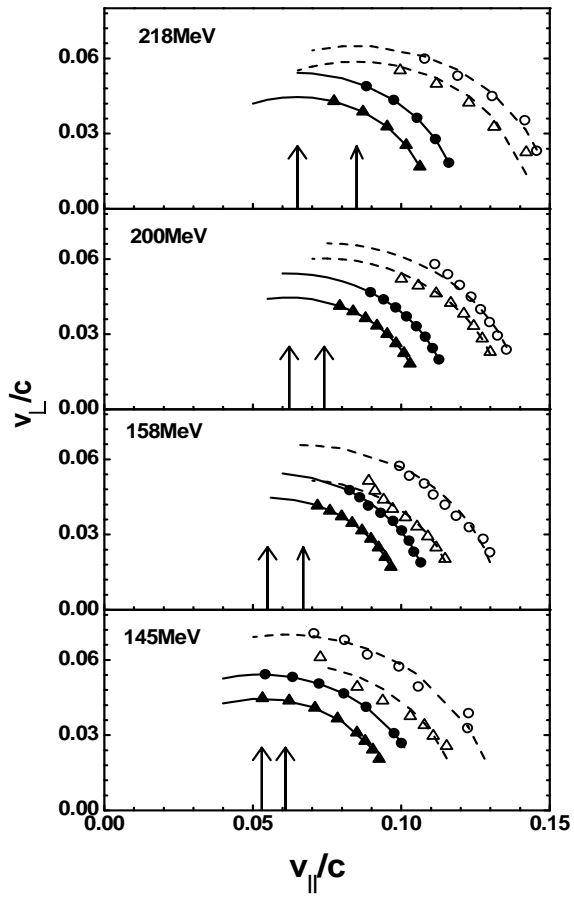


FIG. 6. The average velocities of the fragments Lithium (circle) and Oxygen (triangle) plotted in $v_{||} - v_{\perp}$ plane at different bombarding energies for FF (solid symbol) and DI (open symbol) components. The arrows correspond to the source velocities, v_{CN} (lower) and v_{DI} (higher). The circles correspond to the most probable velocities for FF (solid) and DI (dashed) components.

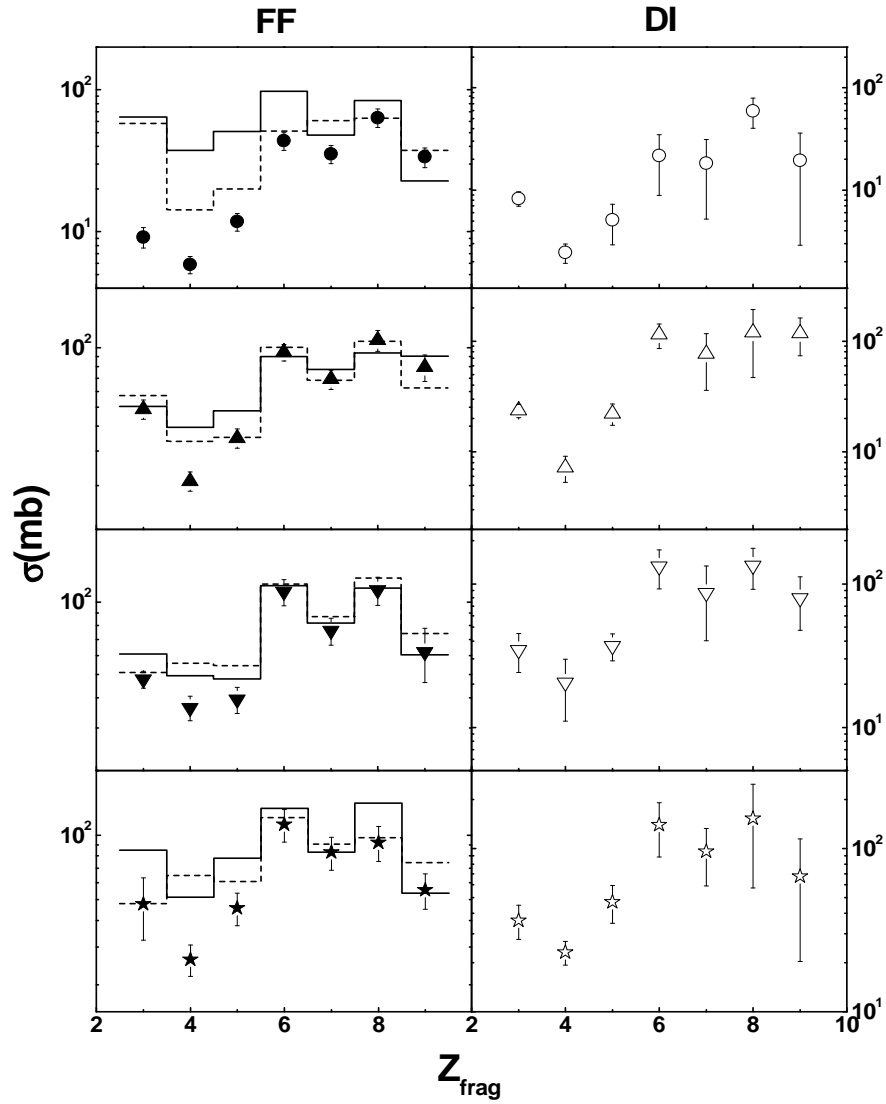


FIG. 7. The total elemental cross-sections of FF (filled symbol) and DI (open symbol) components for $^{20}\text{Ne} + ^{27}\text{Al}$ reaction at the bombarding energies 145 MeV (circle), 158 MeV (triangle), 200 MeV (inverted triangle) and 218 MeV (star), respectively, plotted as a function of fragment charge. The histograms represent the corresponding theoretical predictions using CASCADE (solid) and EHFm (dashed).

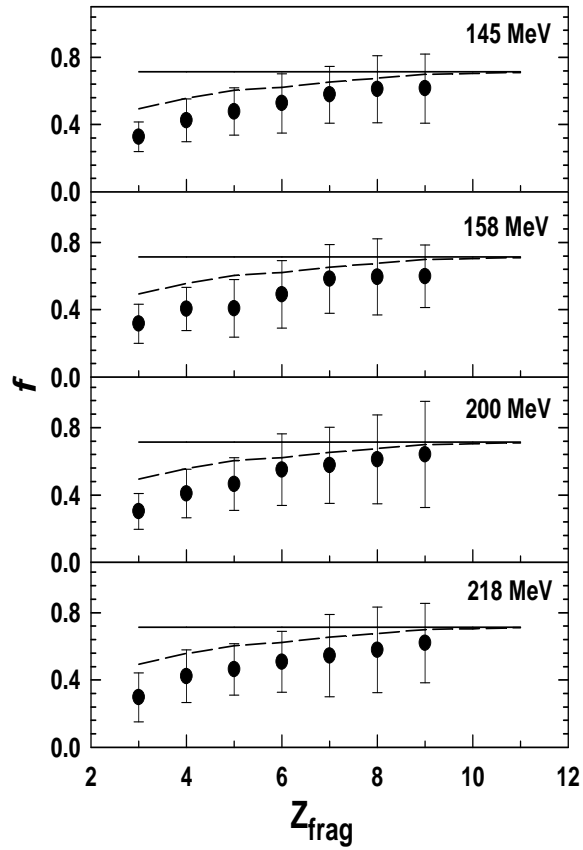


FIG. 8. The angular momentum dissipation factors extracted for different fragments (filled circles) at various incident energies. The corresponding empirical limits are shown by solid (rolling) and dashed (sticking) lines, respectively.

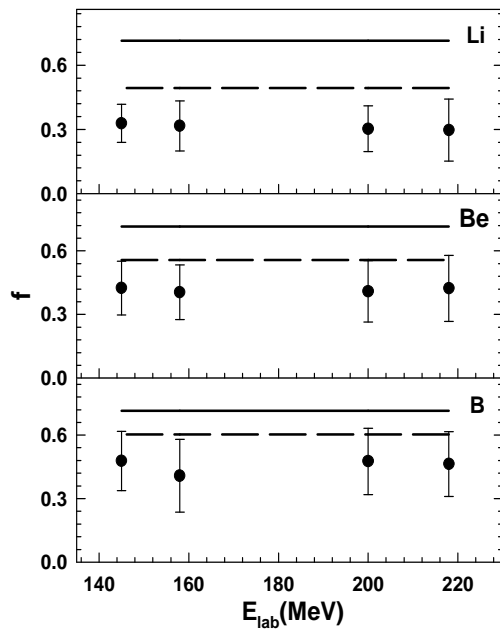


FIG. 9. The variation of angular momentum dissipation factor as a function of incident energy. Filled circles are the experimental estimates; empirical rolling and sticking limits for the same are represented by solid and dashed lines, respectively.